applied sciences

MDPI

Article

Modeling the Dynamic Behavior of a Pilot-Operated Solenoid Valve for an Ultra-High Pressure Vessel

Jaeseong Choi, Jung Hwan Ahn and Hwa Young Kim *

School of Mechanical Engineering, Pusan National University, 2, Busandaehak-ro 63beon-gil, Geumjeong-gu, Busan 46241, Korea; choijaeseong@pusan.ac.kr (J.C.); Jhwahn@pusan.ac.kr (J.H.A.)
* Correspondence: hyokim@pusan.ac.kr; Tel.: +82-51-510-2861

Abstract: A pilot-operated solenoid valve is used to control ultra-high pressure vessels. However, it is difficult to understand its dynamic behavior because the valve operates under ultra-high pressure conditions and the driving unit moves in a multi-step fashion in a tight hidden space. This study aims to identify the system coefficient, especially the damping coefficient, required to analyze the dynamic behavior of a solenoid driving unit. Experiments to measure the dynamic behavior of the driving unit are conducted using two laser sensors and one accelerator. The damping coefficient is estimated using Matlab Simulink, by varying the damping coefficient to match the experimental results. The obtained system coefficients are modeled as equations of motion. It is verified that the valve motion consists of two sequential movements—Phase 1 by pilot plunger and Phase 2 by main plunger, pilot plunger, and the valve initiation time is as fast as 9.9 ms. The damping coefficient of each phase is estimated 0.001 N · s/mm for Phase 1, 0.004 N · s/mm for Phase 2.

Keywords: modeling dynamic behavior; pilot-operated solenoid valve; ultra-high pressure cylinder

Citation: Choi, J.; Ahn, J.H.; Kim, H.Y. Modeling the Dynamic Behavior of a Pilot-Operated Solenoid Valve for an Ultra-High Pressure Vessel. *Appl. Sci.* **2021**, *11*, 2329. https://doi.org/10.3390/app11052329

Academic Editor: José A.F.O. Correia

Received: 26 January 2021
Accepted: 3 March 2021
Published: 5 March 2021

1. Introduction

The solenoid valve controls the flow path by opening or closing the orifice with a plunger, using the attraction force of the solenoid. The solenoid valves are divided into direct-acting valves and pilot-operated valves based on the driving method. Direct-acting valves are valves that contain a single plunger. Owing to their simple driving principle, these valves have the advantage of a fast response. However, when handling high-pressure fluids, the volume occupied by the solenoid valve increases, and the wire burns as a result of the load required to obtain a higher attraction force. Therefore, it is difficult for these mechanisms to control ultra-high pressure fluid forces. As, recently, areas such as hydrogen fuel cell vehicles, hydrogen charging stations require ultra-high pressure fluid control, their importance is being emphasized [1,2]. On the contrary, pilot-operated valves can be used to control ultra-high pressure fluids [3]. A pilot-operated valve consists of a main plunger and a pilot plunger. When the solenoid is magnetized and the pilot plunger is retracted, the structurally connected main plunger is also retracted and the flow path is opened. The pilot-operated valves have the advantage of reducing the fluid force by creating an orifice with a small area in the main plunger itself. As a result, because the outlet orifice can be opened with a small attraction force, and thus, the volume occupied by the solenoid can be reduced and the valve can be miniaturized. However, the response of pilot-operated valves is slow because the flow path is opened in two steps, and it is necessary to wait for the pressure to equalize during the process. In applications such as hydrogen fuel cell vehicles, the dynamic behavior characteristics of these valves is directly related to performance indicators such as the acceleration process of the vehicle. It is necessary to analyze and simulate the behavior characteristics to improve the responsiveness of the system [4].

Kajima calculated theoretically by dividing the magnetic path to simplify the magnetic flux of high-speed solenoid valves used in diesel engines [5]. Piron analyzed the attraction of the valve by adding a Fast-Acting Solenoid Actuator to classical calculation techniques

similar to Kajima for air-gap and bilinear transformation [6]. Liu experimented with the direct acting valve used in CRHDM according to the shape of the contact surface and compared it with the results of ANSYS analysis, but did not identify system variables in the form of equations of motion [7]. Xufeng conducted a study to create a motion equation for dynamic performance analysis of the pilot operated solenoid valve of a spacecraft conversion engine, and analyzed the effect of parameters [8]. Rahman conducted a study to simulate the prediction of the single-phase solenoid plunger position of the PWM method using the SIMON tool [9]. Dai jia analyzed the factors of the system using Matlab Simulink to analyze the dynamic response characteristics of the solenoid valve, including the electro pneumatic valve model and the pneumatic hydraulic valve mode [10]. However, these studies were done for relatively low pressures. Lee designed a pilot-operated solenoid valve for use in ultra-high pressure vessels. However, he did not analyze the dynamic behavior to improve performance [11,12]. Because the valve operates under ultra-high pressure conditions and the drive unit moves in several stages in a tight hidden space. The dynamic motion of plungers is very hard to be investigated.

In this study, the dynamic behavior of the pilot-operated solenoid valve is analyzed with the equation of motion under normal pressure in order to identify the accurate valve actuation time sequence based on measurements of the moving parts of the solenoid, pilot plunger and main plunger, as well as solenoid attraction force. Matlab Simulink is used to compare the experimental results and the simulation results for identifying the damping coefficients.

2. Modeling the Solenoid Motion

2.1. Structure of the Pilot-Operated Solenoid Valve

As shown in Figure 1, the drive unit of the solenoid consists of a pilot plunger, a main plunger, a spring, a spring guide, and a spring seat. The main plunger is connected with a tiny gap (G_p) to a pin of the pilot plunger. Only the pilot plunger is a magnetic substance and starts to move when the core is magnetized, that is Phase 1 of the motion. As the pilot plunger moves the gap (G_p), its pin pulls up the main plunger allowing all parts to move together, that is Phase 2 of the motion.

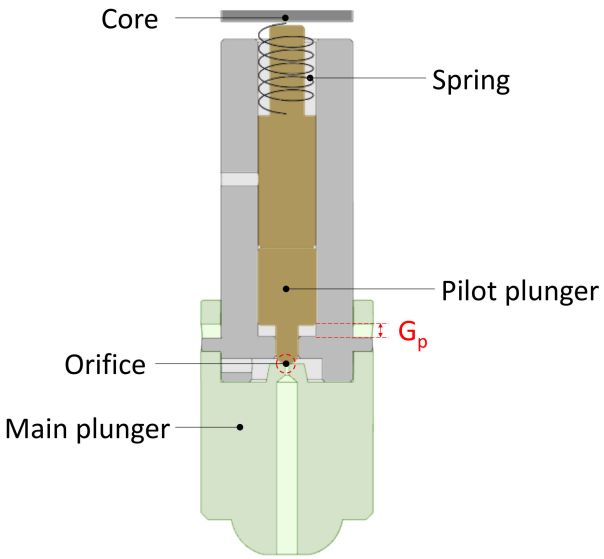

Figure 1. Schematic of the pilot-operated solenoid valve.

2.2. Multi-Step of the Pilot-Operated Solenoid Valve

When DC power is applied to the solenoid coil, magnetizes the core, the solenoid drive unit undergoes Phase 1, 2 motion which makes such multi-step operations as shown in Figure 2. In the initial state, the orifice of the main plunger is closed by the spring in Figure 2a; however, when the attraction force of the solenoid exceeds the fluid force of

the orifice and the elastic force of the spring, the spring seat is retracted and the orifice is opened to allow the fluid between the pilot plunger and the main plunger to escape in Figure 2b. As a result, the inside of the solenoid valve undergoes a pressure equalization process in Figure 2c, and the outlet orifice is completely opened by the attraction force of the solenoid in Figure 2d.

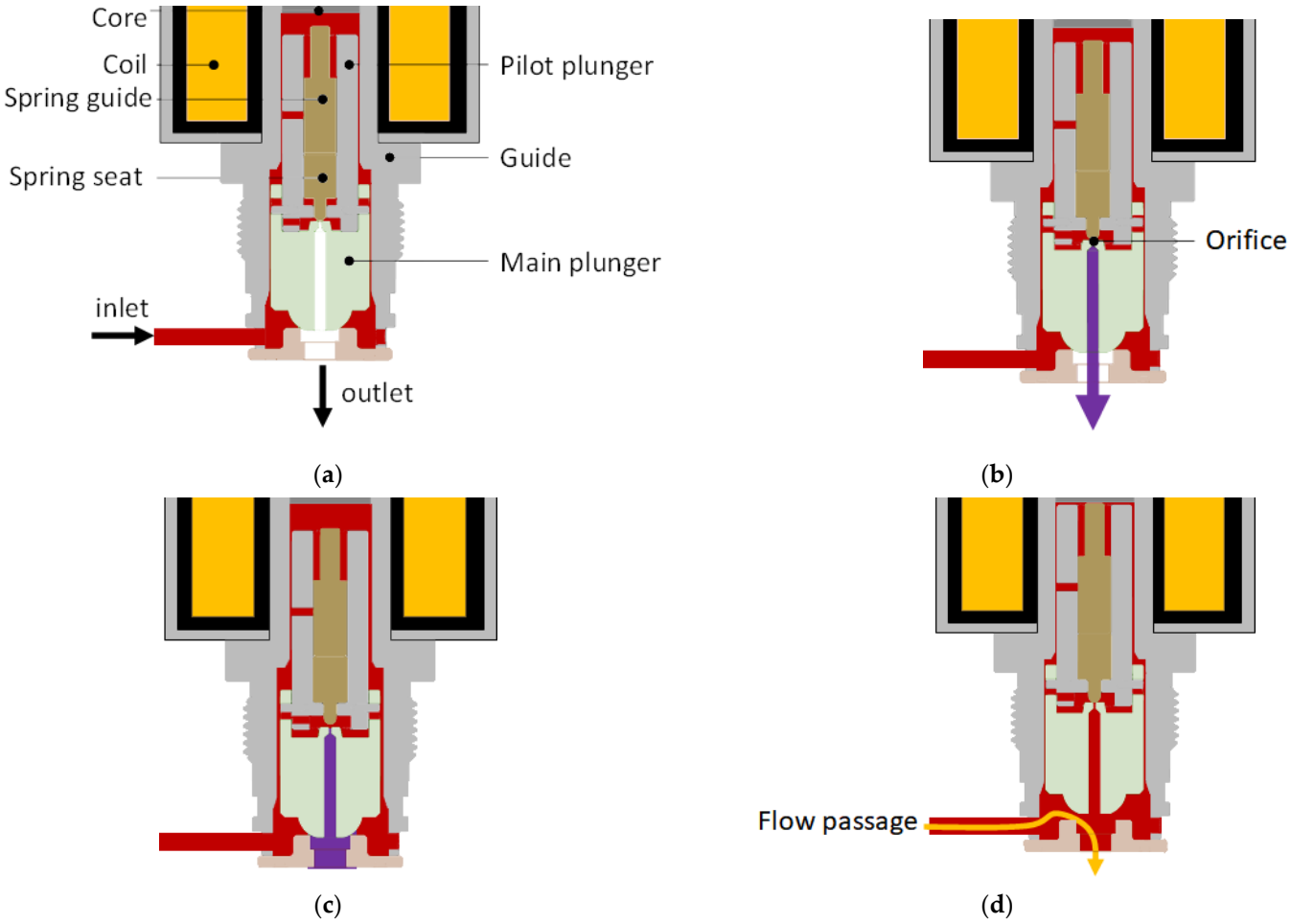

Figure 2. Principle of the pilot-operated solenoid valve: (**a**) initial state; (**b**) application of an electric voltage; (**c**) pressure equilibrium state; (**d**) opening of the flow passage.

2.3. Modeling the Motion Equation by Phase

The solenoid valve can be described as an equation of motion with one degree of freedom because the plunger moves only in the vertical direction. As explained in Section 2.1, the solenoid movement is divided into two Phases. In Phase 1 where only the pilot plunger moves, free body diagram (FBD) is depicted as Figure 3a, while FBD in the second phase as Figure 3b. Where all parameters are: attraction force (F_a), preload force of spring preload (F_p), mass of the pilot plunger (m_p), mass of the main plunger (m_m), mass of the spring seat (m_s), mass of the spring guide (m_g), spring coefficient (k), and damping coefficients (c_1 and c_2).

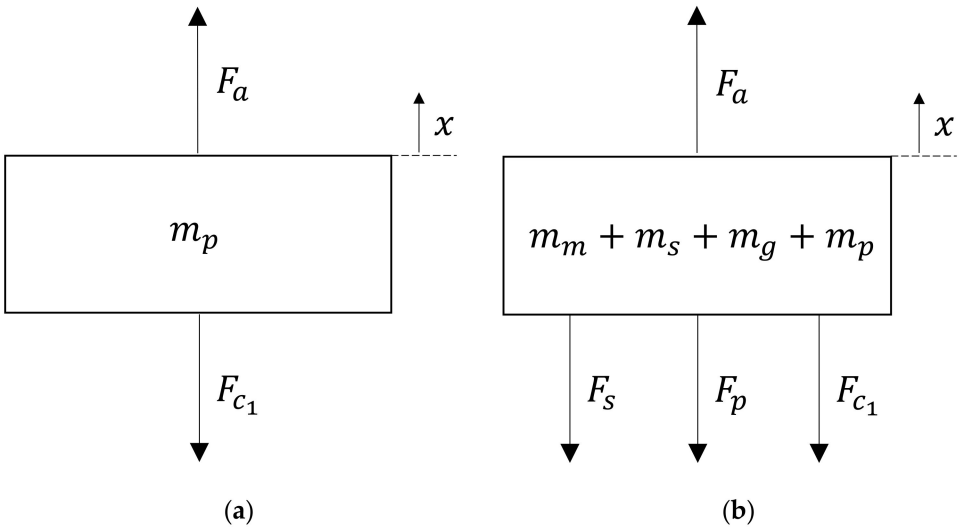

Figure 3. Free body diagram: (**a**) Motion of Phase 1; (**b**) Motion of Phase 2.

In Phase 1, the pilot plunger moves under the influence of the attraction force, and the equation of motion can be written as Equation (1) with the initial conditions Equation (2).

$$m_{\overline{p}}\ddot{x} + c_1\dot{x} = f_a, \text{ for } 0 \leq t < t_1 \tag{1}$$

$$x(0) = 0, \dot{x}(0) = 0. \tag{2}$$

In Phase 2, all the drive unit of the solenoid move together under the influence of the attraction force and the spring preload. The equation of motion can be written as Equation (3) with the initial of Equation (4).

$$(m_p + m_m + m_s + m_g)\ddot{x} + c_2\dot{x} + kx = f_a + f_p, \text{ for } t_1 < t \leq t_2 \tag{3}$$

$$x(t_1) = p_1, x(t_1) = v_1. \tag{4}$$

3. Experiments on the Plunger Movement

3.1. Configuration of the Experiments

Each plunger displacement is measured using a laser displacement sensor, which is installed toward the surface of each plunger. In addition, an accelerometer is installed in the same direction as the solenoid axis to measure the exact position where the pilot plunger hits the main plunger and exact position at which the combined plungers reach at the top. Applying a power of 9 V, sensor signals are acquired through a DAQ board. Table 1 shows the specifications of sensors for the experimental setup, which is shown in Figure 4.

Table 1. Components of the experimental setup.

Equipment	Parameter	Value
Laser sensor (LK-G30, KISTLER)	Measuring range Repeatability	±5 mm 0.05 μm
Accelerometer (8762A10, KISTLER)	Acc. Range Freq. response	±10 G 0.5–6000 Hz

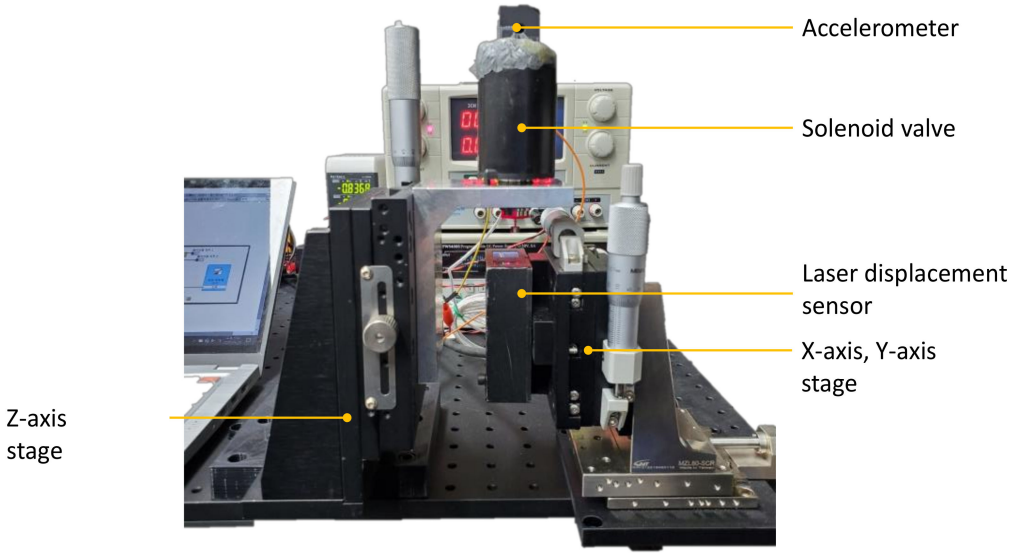

Figure 4. Experimental setup for measuring plunger displacement.

3.2. Experimental Results

The measured displacements are displayed in Figure 5. An even small acceleration occurs at 5.3 ms at which the pilot plunger hits the main plunger. A large acceleration is measured at 9.9 ms at which the combined plungers reach at the top. That is, two-Phase movements are clarified to occur sequentially in 0–5.3 ms and 5.3–9.9 ms. The pilot plunger displacement during Phase 1 is 260 μm and the pilot plunger displacement during Phase 2 is 970 μm. Phase 1 has an average velocity of 49.1 mm/s and Phase 2 has an average velocity of 210.9 mm/s.

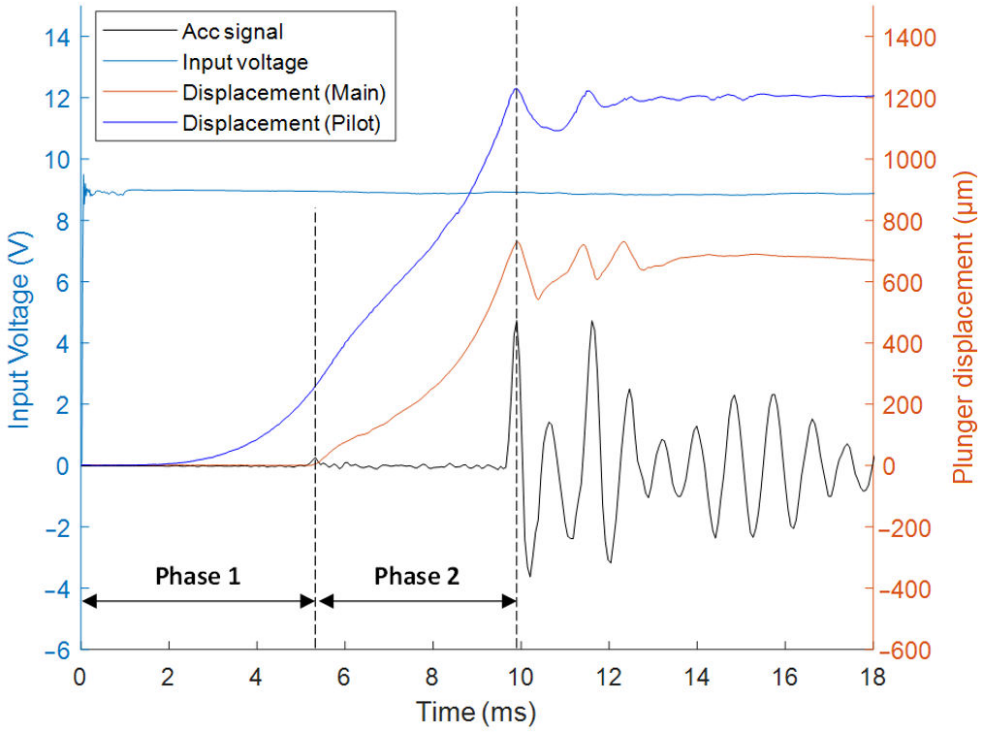

Figure 5. Measured displacements of the pilot plunger and main plunger along operation of the solenoid valve.

4. System Identification through Simulations

4.1. Overview of System Identification

For system identification, the parameters of motion equation such as mass, spring, damping, and external force must be obtained. The mass and spring coefficients are known values. Among the external forces, the attraction force of the solenoid valve can be obtained through experiments. The damping coefficient can be obtained through comparing the experimental results in Section 3.2 and the simulation results, which is obtained is through simulation shown in Figure 6.

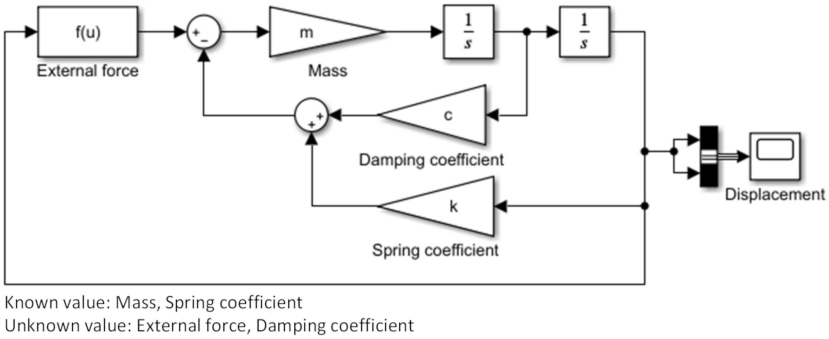

Figure 6. Simulink diagram for simulating the motion of the pilot-operated solenoid valve.

4.2. Attraction Force of Solenoid Valve

The attraction force for opening the flow path is created electromagnetically and its calculation is very difficult due to many unknown parameters as given in Equation (5) [13].

$$f_a = \frac{B^2 S}{2\mu_{air}} \tag{5}$$

In this study, thus, a practical relationship between the attraction force and the air gap distance of the pilot plunger to the core is derived experimentally. The pilot plunger is connected to a load cell, and a linear stage is used to vary the air gap with an accuracy of micrometer using a laser displacement sensor. Table 2 shows the specifications of sensors for the experimental setup, which is shown in Figure 7.

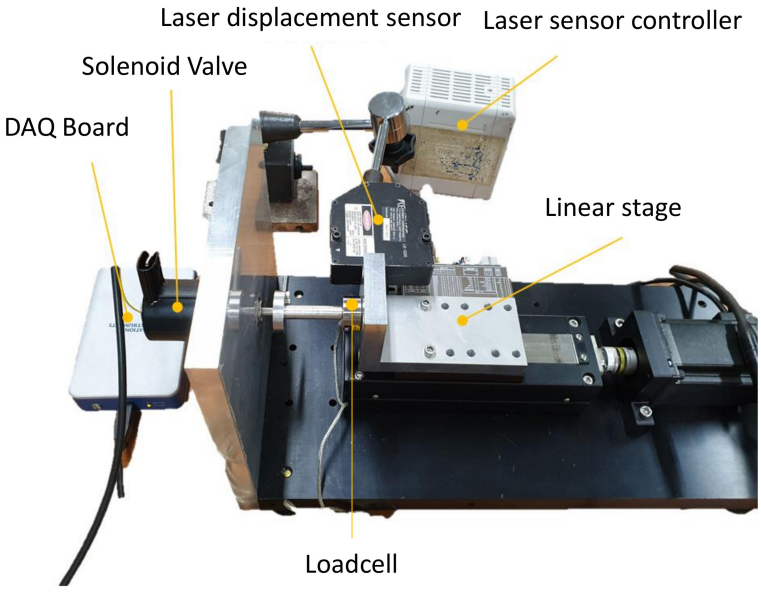

Figure 7. Experimental setup for measuring the attraction force with varying air gap.

Table 2. Components of the experimental setup for measuring the attraction force.

Equipment	Parameter	Value
Laser sensor (LK-G30, KISTLER)	Measuring range	±5 mm
	Repeatability	0.05 µm
Load cell (LCM300, FUTEK)	Rated Output	2 mV/V
	Non-repeatability	±0.25%

The experiment is conducted at 9 V and the results are plotted in Figure 8 with maximum attraction force of 19.1 N. The data is fitted to a third-order polynomial as Equation (6).

$$f_a = 24.026x^3 - 30.931x^2 + 17.096x \quad (6)$$

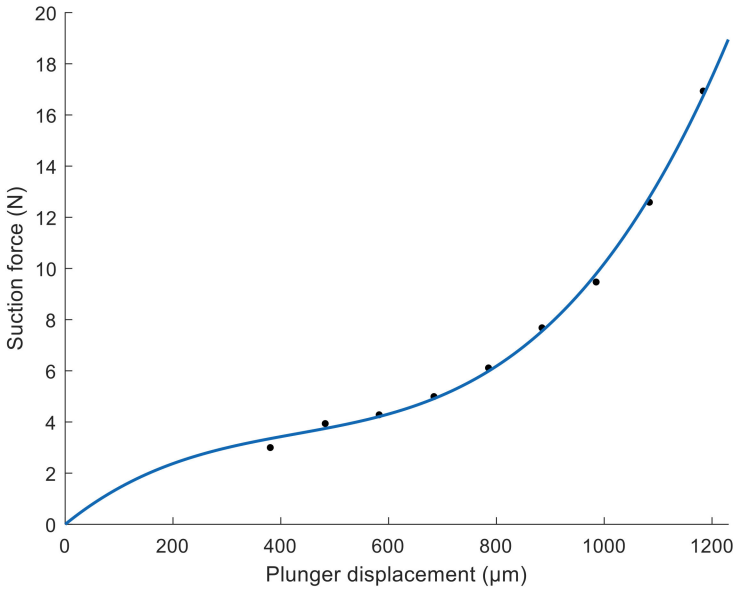

Figure 8. Experimental solenoid attraction force with varying air gap.

4.3. Estimation of the Damping Coefficient

The damping coefficient is estimated through Matlab Simulink, starting from 0 and increasing by 0.0001 to find a value consistent with the experimental results. The Runge–Kutta model which is widely used for electromagnetic analysis with high accuracy is applied as solver [14].

The damping coefficient c_1 is 0.001 N · s/mm for Phase 1, the damping coefficient c_2 is 0.004 N · s/mm for Phase 2. The damping coefficient c_2 is four times greater than the damping coefficient of c_1, due to the effect of viscous friction on the fluid flow through the orifice.

4.4. Motion Equation for the Pilot-Operated Solenoid Valve

The equation of motion is completed based on Equations (1) and (3) by substituting mass, spring, damping, and external force for each phase described in Equations (7) and (8).

$$0.109\ddot{x} + 0.001\dot{x} = 24.026x^3 - 30.931x^2 + 17.096x, \text{ for } 0 \leq t \leq t_1 \quad (7)$$

$$0.134\ddot{x} + 0.004\dot{x} + 0.428x = 24.026x^3 - 30.931x^2 + 17.096x - 2.524, \text{ for } t_1 \leq t \leq t_2 \quad (8)$$

The simulation results are compared with the experimental results at a total of 1230 µm for 9.9 ms in Figure 9. The simulation results showed an error of 17 µm at entire displacement compared to the experimental results. Therefore, the equation of motion is reliable.

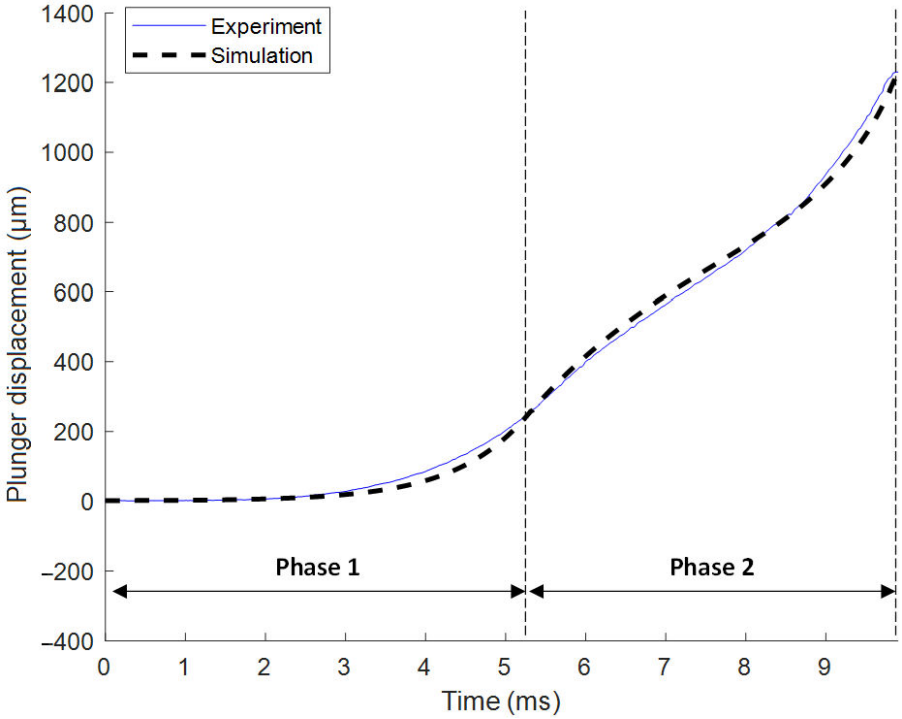

Figure 9. Comparison of displacements between the test and simulation.

5. Conclusions

Dynamic behavior of the driving unit in a pilot-operated solenoid valve for an ultra-high pressure vessel is analyzed through experiments, simulation, and system identification. The analyzed results are modeled as an equation of motion. The new findings are as follows.

1. The driving unit motion consists of two sequential movements. In Phase 1, only pilot plunger moves, and in Phase 2, pilot plunger and main plunger move together. The mathematical models for the driving unit are constructed.
2. Phase 1 has a displacement of 260 μm over 5.3 ms, with an average velocity of 49.1 mm/s. Phase 2 has a displacement of 970 μm over 4.6 ms, with an average velocity of 210.9 mm/s. Although Phase 2 has a large mass and high damping coefficient, the average velocity is four times faster, so the influence of the attraction force is dominant.
3. The damping coefficient of each phase is estimated 0.001 N · s/mm at Phase 1, 0.004 N · s/mm at Phase 2 by comparing the experimental results and the simulation results through Matlab Simulink.

Author Contributions: Conceptualization, J.C. and J.H.A.; Formal analysis, J.C. and H.Y.K.; Methodology, J.C. and J.H.A.; Resources, J.H.A.; Software, J.C.; Supervision, J.H.A. and H.Y.K.; Validation, J.C.; Writing—original draft, J.C.; Writing—review & editing, J.H.A. and H.Y.K.; All authors have read and agreed to the published version of the manuscript.

Funding: This work was supported by a two year research Grant of Pusan National University.

Institutional Review Board Statement: Not applicable.

Informed Consent Statement: Not applicable.

Data Availability Statement: Not applicable.

Conflicts of Interest: The authors declare no conflict of interest.

References

1. Ahn, B.K. Development trend of the Clean Tech Fuel Cell Vehicles. *Korean Soc. Mech. Eng.* **2012**, *52*, 34–38.
2. Li, M.; Bai, Y.; Zhang, C.; Song, Y.; Jiang, S.; Grouset, D.; Zhang, M. Review on the Research of Hydrogen Storage System Fast Refueling in Fuel Cell Vehicle. *Int. J. Hydrog. Energy* **2019**, *44*, 10677–10693. [CrossRef]
3. Asano, S.; Ozaki, H.; Kato, K.; Wada, M. Development of In-Tank Solenoid Valve Compatible with 70 MPa High-Pressure Hydrogen Storage and Supply System for FCV. *Honda R&D Tech. Rev.* **2016**, *28*, 8–14.
4. Lansky, Z.J. *Industrial Pneumatic Control*; CRC Press: Boca Raton, FL, USA, 1986; pp. 54–62.
5. Kajima, T.; Kawamura, Y. Development of a High-Speed Solenoid Valve: Investigation of Solenoids. *IEEE Trans. Ind. Electron.* **1995**, *42*, 1–8. [CrossRef]
6. Piron, M.; Sangha, P.; Reid, G.; Miller, T.J.E.; Ionel, D.M. Rapid Computer-Aided Design Method for Fast-Acting Solenoid Actuators. *IEEE Trans. Ind. Applicat.* **1999**, *35*, 991–999. [CrossRef]
7. Liu, Q.; Bo, H.; Qin, B. Experimental Study and Numerical Analysis on Electromagnetic Force of Direct Action Solenoid Valve. *Nucl. Eng. Des.* **2010**, *240*, 4031–4036. [CrossRef]
8. Xufeng, F.; Changbin, G.; Zhenxing, W. Dynamic Performance Analysis of a Pilot Operated Solenoid Valve in a Divert Engine for Spacecrafts. In Proceedings of the 2019 IEEE 8th International Conference on Fluid Power and Mechatronics (FPM), Wuhan, China, 10–13 April 2019; pp. 575–578.
9. Rahman, M.F.; Cheung, N.C.; Lim, K.W. Position Estimation in Solenoid Actuators. *IEEE Trans. Ind. Applicat.* **1996**, *32*, 552–559. [CrossRef]
10. Dai Jia, H.M.; Yong, Y.; Hengwei, Z.; Jiaqing, M. Simulation on the Dynamic Response Characteristics of Solenoid Valve. *J. Rocket Propuls.* **2007**, *1*, 40–48.
11. Lee, H.R.; Ahn, J.H.; Kim, H.Y. Design of a solenoid actuator for a cylinder valve in a fuel cell vehicle. *Appl. Sci.* **2016**, *6*, 288. [CrossRef]
12. Lee, H.R.; Ahn, J.H.; Shin, J.O.; Kim, H.Y. Design of Solenoid Actuator for FCV Cylinder Valve Considering Structural Safety. *J. Korean Soc. Manuf. Technol. Eng.* **2016**, *25*, 157–163. [CrossRef]
13. Roters, H.C. *Electromagnetic Devices*; Wiley: New York, NY, USA, 1941; pp. 130–149.
14. Shampine, L.F.; Reichelt, M.W. The matlab ode suite. *SIAM J. Sci. Comput.* **1997**, *18*, 1–22. [CrossRef]